AIAA 81-0192R

Three-Dimensional Supersonic Viscous Flow over a Cone at Incidence

A. Lin* and S. G. Rubin†
University of Cincinnati, Cincinnati, Ohio

The viscous supersonic flow over a sharp cone with half-angle θ and at incidence angles $\alpha/\theta \leq 5.4$ is examined numerically. The parabolized Navier-Stokes (PNS) equations are differenced in a boundary layer-like manner and evaluated by a marching technique. The coupled strongly implicit procedure (CSIP) is constructed in a new $(2\times 2)+1$ form in order to evaluate the coupled axial and azimuthal momentum equations, continuity equation and Rankine-Hugoniot shock relations. The method is designed for large incidence calculations; however, symmetry conditions are imposed at the wind and lee planes for computational simplicity. This condition may artificially suppress vortex shedding or "instability" at the larger incidence angles. Although upstream influence is essentially negligible for the present geometry, a global relaxation procedure for the pressure interaction, previously developed for incompressible flow, is tested on the cone geometry. It is shown that departure effects can be eliminated for arbitrarily small axial stepsize by forward differencing of the axial pressure gradient. This approximation retains the implicit free pressure interaction required for other geometries where axial flow separation is possible. Incompressible separated flow problems have previously been examined in this manner, but the present compressible flow consideration is unique.

I. Introduction

FOR a significant class of geometric configurations and flow conditions solutions of the full Navier-Stokes equations can be approximated quite accurately with boundary-layer like marching techniques in thin viscous layers, coupled with relaxation or marching procedures for inviscid sub- and supersonic regions, respectively. For large Reynolds number flows this approach has been developed in several ways, e.g., interacting boundary-layer theory,[1] parabolized Navier-Stokes (PNS) theory,[2,8] viscous or single layer theory[3] and two-layer interactive theory.[4,12] Single sweep marching for supersonic outer flows with little or no upstream interaction, and global or multiple pass methods when upstream influence is an important feature of the flow, including possible separation, have been discussed for a variety of problems. References 2 and 3 review much of the earlier work on this subject.

The present study is concerned with a single sweep PNS application for the supersonic laminar flow over a sharp cone geometry and the extension to a multisweep or global procedure for the Navier-Stokes equations. This geometry has been examined extensively during the past decade and, in view of the variety of complex flow phenomena associated with the cone at incidence, it has served as a prototype for analysis of new computational methods. Of particular interest here are procedures that allow for the evaluation of such a configuration at relatively large angles of incidence. In particular, we are concerned with the accurate prediction of the secondary flow vortex patterns, imbedded shock formation, axial and secondary flow pressure interaction, and, finally, the surface pressure and heat transfer.

The secondary flow interaction with shocks and vortex formation is numerically nontrivial. A coupled strongly implicit (CSIP) algorithm, developed previously for the incompressible Navier-Stokes equations,[5] is applied here in order to provide a "two-dimensional" coupling for the three velocity components. The secondary flow pressure and temperature gradients remain uncoupled in order to limit computer storage requirements; however, the latter is evaluated with the strongly implicit (SIP) algorithm. The outer shock boundary conditions are completely coupled into the CSIP algorithm.[6]

The continuity and normal momentum equations are related through the differencing and the algorithm to the evaluation of the normal velocity and pressure, respectively. This is contrary to most conventional Navier-Stokes and PNS procedures. However, it is consistent with the boundary layer and thin shock layer approaches that have been applied in noninteractive analyses.

As a peripheral aspect of the present study, several difference approximations for the axial pressure gradient term p_ξ appearing in the ξ-momentum equation are considered. This term controls the "elliptic" pressure interaction[2,8] and can produce the so-called departure "instability" indicative of the upstream pressure effect. It can be shown that with an appropriate forward difference approximation to p_ξ, the departure effect can be suppressed. The resultant consistent, stable, pressure interaction procedure, tested previously for incompressible flows,[2,8] will be shown to be applicable also for the cone calculations. Since there is no strong upstream interaction for the sharp cone geometry this has little effect on the solutions; however, it does provide a basis for further consideration with other configurations.

Solutions are presented for several cases; however, the major emphasis here is on the Tracy 10-deg half-angle cone[7] and the Marcillat[9] 9-deg half-angle cone. Incidence angles of from 0 to 54 deg are considered.

II. Governing Equations

The full steady Navier-Stokes equations are considered for the global relaxation procedure. However, for the infinite cone geometry considered here, only a single marching sweep is in fact required as upstream interaction is negligible. Therefore, the axial diffusion terms have not been introduced.

Presented as Paper 81-0192 at the AIAA 19th Aerospace Sciences Meeting, St. Louis, Mo., Jan. 12-15, 1981; submitted Feb. 20, 1981; revision received Feb. 1, 1982.

*Research Assistant Professor, Dept. of Aerospace Engineering and Applied Mechanics. Member AIAA.

†Professor, Dept. of Aerospace Engineering and Applied Mechanics. Associate Fellow AIAA.

A surface oriented coordinate system is considered (Fig. 1); x is measured along the cone generators; y is normal to the surface, and ϕ is the circumferential or azimuthal angle; $\phi = 0$, π at the wind and lee planes, respectively.

In this coordinate frame the governing conservation equations are as follows.

Continuity:

$$\frac{\partial \rho}{\partial t} + \frac{\partial}{\partial x}(\rho u) + \frac{\partial}{\partial y}(\rho v) + \frac{1}{r}\frac{\partial}{\partial \phi}(\rho w) + \frac{\rho}{r}(u\sin\theta + v\cos\theta) = 0 \tag{1a}$$

x momentum:

$$\frac{\partial u}{\partial t} + u\frac{\partial u}{\partial x} + v\frac{\partial u}{\partial y} + \frac{w}{r}\frac{\partial u}{\partial \phi} - \frac{w^2\sin\theta}{r} = -\frac{1}{\rho}\frac{\partial P}{\partial x} + \frac{1}{\rho}\left\{\frac{4}{3}\frac{\partial}{\partial x}\left(\mu\frac{\partial u}{\partial x}\right) - \frac{2}{3}\frac{\partial}{\partial x}\left(\mu\frac{\partial v}{\partial y}\right) + \frac{\partial}{\partial y}\left(\mu\frac{\partial v}{\partial x}\right) + \frac{\partial}{\partial y}\left(\mu\frac{\partial u}{\partial y}\right) + \frac{1}{r^2}\frac{\partial}{\partial \phi}\left(\mu\frac{\partial u}{\partial \phi}\right)\right.$$
$$-\left(\frac{2}{3r}\frac{\partial u}{\partial x} + \frac{4\mu}{3r}\sin\theta\right)(u\sin\theta + v\cos\theta) + \frac{4\sin\theta}{3r}\mu\frac{\partial u}{\partial x} + \frac{\mu\cos\theta}{r}\frac{\partial u}{\partial y} + \frac{\mu\cos\theta}{3r}\frac{\partial v}{\partial x} + \frac{1}{r}\frac{\partial \mu}{\partial \phi}\frac{\partial w}{\partial x} - \left(\frac{7\sin\theta}{3r^2}\mu + \frac{2}{3r}\frac{\partial \mu}{\partial x}\right)\frac{\partial w}{\partial \phi}$$
$$\left. + \frac{\mu}{3r}\frac{\partial^2 w}{\partial x \partial \phi} - \frac{\sin\theta}{r^2}\frac{\partial \mu}{\partial \phi}w\right\} \tag{1b}$$

y momentum:

$$\frac{\partial v}{\partial t} + u\frac{\partial v}{\partial x} + v\frac{\partial v}{\partial y} + \frac{w}{r}\frac{\partial v}{\partial \phi} - \frac{w^2\cos\theta}{r} = -\frac{1}{\rho}\frac{\partial P}{\partial y} + \frac{1}{\rho}\left\{\frac{4}{3}\frac{\partial}{\partial y}\left(\mu\frac{\partial v}{\partial y}\right) + \frac{\partial}{\partial x}\left(\mu\frac{\partial v}{\partial x}\right) + \frac{\partial \mu}{\partial x}\frac{\partial u}{\partial y} - \frac{2}{3}\frac{\partial \mu}{\partial y}\frac{\partial u}{\partial x} + \frac{\mu}{3}\frac{\partial^2 u}{\partial x \partial y} + \frac{1}{r^2}\frac{\partial}{\partial \phi}\left(\mu\frac{\partial v}{\partial \phi}\right)\right.$$
$$+\frac{4\mu\cos\theta}{3r}\frac{\partial v}{\partial y} + \frac{\mu\sin\theta}{r}\frac{\partial v}{\partial x} - \frac{4\mu\cos\theta}{3r^2}(u\sin\theta + v\cos\theta) - \frac{2\sin\theta}{3r}\frac{\partial \mu}{\partial y}u + \frac{\mu\sin\theta}{3r}\frac{\partial u}{\partial y} - \frac{2\cos\theta}{3r}\frac{\partial \mu}{\partial y}v + \frac{1}{r}\frac{\partial \mu}{\partial \phi}\frac{\partial w}{\partial y}$$
$$\left. - \left(\frac{7\mu\cos\theta}{3r^2} + \frac{2}{3r}\frac{\partial \mu}{\partial y}\right)\frac{\partial w}{\partial \phi} + \frac{\mu}{3r}\frac{\partial^2 w}{\partial y \partial \phi} - \frac{\cos\theta}{r^2}\frac{\partial u}{\partial \phi}w\right\} \tag{1c}$$

ϕ momentum:

$$\frac{\partial w}{\partial t} + u\frac{\partial w}{\partial x} + v\frac{\partial w}{\partial y} + \frac{w}{r}\frac{\partial w}{\partial \phi} + \frac{w}{r}(u\sin\theta + v\cos\theta) = -\frac{1}{\rho r}\frac{\partial P}{\partial \phi} + \frac{1}{\rho}\left\{\frac{\partial}{\partial x}\left(\mu\frac{\partial w}{\partial x}\right) + \frac{\partial}{\partial y}\left(\mu\frac{\partial w}{\partial y}\right) + \frac{4}{3r^2}\frac{\partial}{\partial \phi}\left(\mu\frac{\partial w}{\partial \phi}\right) + \frac{1}{r}\frac{\partial \mu}{\partial x}\frac{\partial u}{\partial \phi}\right.$$
$$+\frac{1}{r}\frac{\partial \mu}{\partial y}\frac{\partial v}{\partial \phi} - \frac{2}{3r}\frac{\partial \mu}{\partial \phi}\left(\frac{\partial u}{\partial x} + \frac{\partial v}{\partial y}\right) + \frac{\mu}{3r}\left(\frac{\partial^2 u}{\partial x \partial \phi} + \frac{\partial^2 v}{\partial y^2}\right) + \frac{7\mu}{3r^2}\left(\frac{\partial u}{\partial \phi}\sin\theta + \frac{\partial v}{\partial \phi}\cos\theta\right) + \frac{4}{3r^2}\frac{\partial \mu}{\partial \phi}(u\sin\theta + v\cos\theta)$$
$$\left. + \frac{\mu}{r}\left(\frac{\partial w}{\partial x}\sin\theta + \frac{\partial w}{\partial y}\cos\theta\right) - \left(\frac{\mu}{r^2} + \frac{\cos\theta}{r}\frac{\partial \mu}{\partial y} + \frac{\sin\theta}{r}\frac{\partial \mu}{\partial x}\right)w\right\} \tag{1d}$$

Energy equation:

$$\rho\frac{\partial}{\partial t}(C_pT) + \rho u\frac{\partial}{\partial x}(C_pT) + \rho v\frac{\partial}{\partial y}(C_pT) + \frac{\rho w}{r}\frac{\partial}{\partial \phi}(C_pT) = \frac{\partial P}{\partial t} + u\frac{\partial P}{\partial x} + v\frac{\partial P}{\partial y} + \frac{w}{r}\frac{\partial P}{\partial \phi} + \frac{\partial}{\partial x}\left(k\frac{\partial T}{\partial x}\right) + \frac{\partial}{\partial y}\left(k\frac{\partial T}{\partial y}\right)$$
$$+\frac{1}{r}\frac{\partial}{\partial \phi}\left(\frac{k}{r}\frac{\partial T}{\partial \phi}\right) + \frac{k}{r}\left(\frac{\partial T}{\partial x}\sin\theta + \frac{\partial T}{\partial y}\cos\theta\right) + \frac{4\mu}{3}\left[\left(\frac{\partial u}{\partial x}\right)^2 + \left(\frac{\partial v}{\partial y}\right)^2 - \frac{\partial u}{\partial x}\frac{\partial v}{\partial y}\right] + \frac{4\mu}{3r^2}\left[u\sin\theta + v\cos\theta + \frac{\partial w}{\partial \phi}\right]^2$$
$$+\mu\left(\frac{\partial u}{\partial y} + \frac{\partial v}{\partial x}\right)^2 + \mu\left[\left(\frac{1}{r}\frac{\partial u}{\partial \phi} + \frac{\partial w}{\partial x} - \frac{w\sin\theta}{r}\right)^2 + \left(\frac{1}{r}\frac{\partial v}{\partial \phi} + \frac{\partial w}{\partial y} - \frac{w\cos\theta}{r}\right)^2\right] - \frac{4\mu}{3r}\left(u\sin\theta + v\cos\theta + \frac{\partial w}{\partial \phi}\right)\left(\frac{\partial u}{\partial x} + \frac{\partial v}{\partial y}\right) \tag{1e}$$

where θ is the half-cone angle and $r = x\sin\theta + y\cos\theta$. In addition, the state equation and viscosity-temperature and thermal conductivity-temperature relations close the system. The Sutherland law is used for $\mu = \mu(T)$ and the Prandtl number $Pr = \mu c_p/k$ is constant.

The system Eq. (1) is nondimensionalized with the shock-layer thickness $\delta(x,\phi)$ so that $\eta = y/\delta$; $\xi = x$ and $\Phi = \phi$. The velocities are normalized with the freestream U_∞, ρ with ρ_∞, p with $\rho_\infty U_\infty^2$, and T with $U_\infty^2/C_{p\infty}$. The unit Reynolds number is defined as $Re = \rho_\infty U_\infty/\mu_\infty$. Equations (1) are then transformed from (x,y,Φ) to (ξ,η,ϕ) coordinates. The respective velocities are (u,v,w). The derivatives in the (x,Φ) plane are transformed to the (ξ,Φ) plane as follows.

$$\frac{\partial}{\partial x} = \frac{\partial}{\partial \xi} - \frac{\eta}{\delta}\delta_\xi\frac{\partial}{\partial \eta} \tag{2a}$$

and

$$\frac{\partial}{\partial \phi} = \frac{\partial}{\partial \Phi} - \frac{\eta}{\gamma\delta}\delta_\phi\frac{\partial}{\partial \eta} \tag{2b}$$

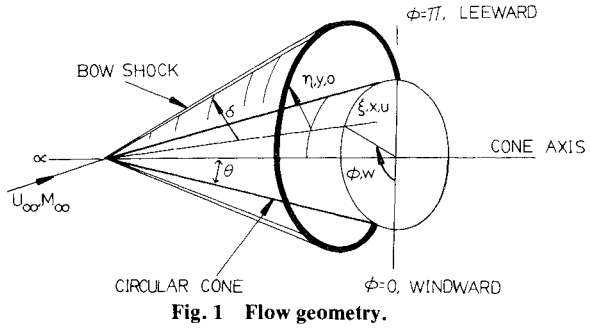

Fig. 1 Flow geometry.

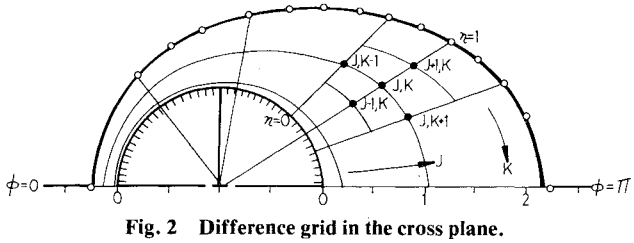

Fig. 2 Difference grid in the cross plane.

Although the pressure appears to be uncoupled from the (u,v,w) CSIP algorithm, the p_x and p_ϕ terms do couple partially through the p_η contributions in Eq. (2). This contribution can be eliminated, with the normal momentum equation, Eq. (1c), in terms of (u,v,w). In fact, for inviscid conical flow, $\partial/\partial\xi \equiv 0$ and, therefore, we would expect the role of p_ξ to be relatively minor. The other ξ derivatives are not negligible in the boundary layer and most probably are important in the outer portion of the shock layer for larger incidence angles. The final system of equations is quite formidable and is given in Ref. 6.

III. Difference Equations

The transformed equations are differenced as follows. For the axial (ξ) and azimuthal (Φ) momentum equations, central differencers are used for the η and Φ derivativer and upwind differencers are used for the ξ derivative (see Fig. 2).

The continuity and normal momentum equations, as noted previously, are considered in the boundary layer or thin shock layer manner as first-order equations for v and p, respectively, and are differenced at the half-point $\eta_j + (\Delta\eta/2)_j$ with the trapezoidal rule. When the p_η term from the η momentum equation is used in Eqs. (2a) and (2b), conventional central differences are applied for the coupled velocity derivatives that are introduced into the ξ and ϕ momentum equations. The final system of difference equations are quasilinearized to provide the familiar second-order approximation.

IV. Numerical Algorithm and Solution Procedure

After differencing, substitution of p_η, and quasilinearization, the final system to be evaluated is of the following form for (u,v,w) at $\xi = \xi_i$.

ξ, ϕ momentum:

$$E_{\ell u_{j,k}} U_{j+1,k} + W_{\ell u_{j,k}} U_{j-1,k} + N_{\ell u_{j,k}} U_{j,k+1} + S_{\ell u_{j,k}} U_{j,k-1} + P_{\ell u_{j,k}} U_{j,k} + E_{\ell w_{j,k}} W_{j+1,k} + W_{\ell w_{j,k}} W_{j-1,k} + N_{\ell w_{j,k}} W_{j,k+1} + S_{\ell w_{j,k}} W_{j,k-1} + P_{\ell w_{j,k}} W_{j,k} + W_{\ell v_{j,k}} V_{j-1,k} + P_{\ell v_{j,k}} V_{j,k} + E_{\ell v_{j,k}} V_{j+1,k} + F_{\ell j,k} = 0 \quad (3a)$$

where $\ell = 2, 3$ for ξ, ϕ equations, respectively.

Continuity:

$$V_{j,k} = W_{1v_{j,k}} V_{j-1,k} + P_{1u_{j,k}} u_{j,k} + W_{1u_{j,k}} U_{j-1,k} + P_{1w_{j,k}} W_{j,k} + W_{1w_{j,k}} W_{j-1,j} + N_{1w_{j,k}} W_{j,k+1} + S_{1w_{j,k}} W_{j,j-1} + WN_{1w_{j,k}} W_{j-1,k+1} + WS_{1w_{j,k}} W_{j-1,k-1} + F_{1_{j,k}} = 0 \quad (3b)$$

The coupled strongly implicit (CSIP) algorithm is of the form[5]

$$U_{j,k} = A_{11_{j,k}} U_{j-1,k} + A_{12_{j,k}} U_{j,k+1} + B_{11_{j,k}} W_{j-1,k} + B_{12_{j,k}} W_{j,k+1} + C_{1_{j,k}} V_{j-1,k} + D_{1_{j,k}} \quad (4a)$$

$$W_{j,k} = A_{21_{j,k}} U_{j-1,k} + A_{22_{j,k}} U_{j,k+1} + B_{21_{j,k}} W_{j-1,k} + B_{22_{j,k}} W_{j,k+1} + C_{2_{j,k}} V_{j-1,k} + D_{2_{j,k}} \quad (4b)$$

and the continuity equation, Eq. (3b), where the corner points $W_{j-1,k\pm1}$ are treated implicitly. The algorithm is structured to evaluate all k values before proceeding from j to $j+1$.

This is a $(2\times2)+1$ matrix system and not the much larger (u,v,w) 3×3 system. The algorithm Eqs. (4a) and (4b) are used in Eqs. (3a) and (3b) to eliminate $U_{j+1,k}$, $W_{j+1,k}$, $U_{j,k-1}$, and $W_{j,k-1}$. See Ref. 5 for a matrix description of the CSIP algorithm, which is obtained by directly relating Eqs. (3a) and (3b) to Eqs. (4a) and (4b). The recursion relationships are given in Ref. 6. The final system Eq. (4) is obtained as follows. 1) The term $v_{j+1,k}$ appearing in the two momentum equations [Eq. (3a) with $\ell = 2,3$] is eliminated with continuity Eq. (3b) evaluated at the point $j+\frac{1}{2}$. A second substitution in Eq. (3a) is used for $v_{j,k}$ in terms of $v_{j-1,k}$, i.e., the continuity equation is now differenced at the point $j-\frac{1}{2}$. 2) The strongly implicit algorithm [Eqs. (4a) and (4b)] is then used to restructure the momentum equations by eliminating the terms $u_{j+1,k}$, $u_{j,k-1}$, $w_{j+1,k}$, and $w_{j,k-1}$; a similar substitution is used in the continuity equation to eliminate the term $w_{j,k-1}$. It should be noted that this algorithm requires that the v_ϕ contributions be treated iteratively. Since v_ϕ appears only in the ϕ momentum equation and only as a viscous contribution, this explicit effect will not affect significantly the convergence rate. The boundary conditions for u, v, w, to be discussed in the following section, are coupled implicitly into the CSIP algorithm. During the iterations of the CSIP algorithm, the thermodynamic variables, viscosity coefficient, and circumferential pressure gradient are fixed. In addition, the shock stand-off distance δ and certain δ derivatives are also treated explicitly everywhere except at the shock boundary where these conditions are coupled implicitly into the algorithm (see Ref. 6).

The energy equation, which is of the form (3a), is solved independently with a SIP algorithm which is similar to Eq. (49) of Ref. 6. The pressure is obtained from the transformed normal momentum Eq. (1c) by integrating from the shock to the surface with the trapezoidal rule.

The rate of convergence of each CSIP step is very rapid. For the overall marching procedure, the convergence rate is, however, limited by the iteration required for the thermodynamic variables and the azimuthal shock displacement derivative δ_ϕ. Although some additional coupling of the energy and normal momentum equation is possible in order to alleviate the former situation, the δ_ϕ iteration would remain a problem. The stability of the iterative procedure for δ_ϕ is in many ways similar to that found for p_ξ in the global pressure analysis.

This describes completely the evaluation at each location $\xi = \xi_i$ for the single sweep marching procedure. If the additional sweeps are necessary, i.e., when pressure interaction and upstream influence are important, the process is repeated from the initial $\xi = \xi_0$ location. The forward p_ξ difference

terms and the axial diffusion and correctors, if these terms are included in the calculation, are updated at this time. Multiple pass calculations have only been considered to a limited extent for the cone geometry and these will be discussed later in this paper.

V. Boundary and Initial Conditions

Initial conditions are generally obtained at a point $\xi=\xi_0$ near the cone tip directly from the governing difference equations by assuming uniform conditions or by applying the numerical algorithm with $\partial/\partial\xi\equiv 0$; i.e., a conical flow approximation. Inviscid or step profiles with no-slip surface conditions are also assumed to start this calculation. This procedure appears to work quite well for incidence angles up to $\alpha/\theta\approx 2.5$. For moderate α/θ, the effect of all initial conditions appears to be minimal. It should be noted that although the $\partial/\partial\xi=0$ solutions may be reasonable approximations for the cone geometry,[13] the exact solutions are in fact noticeably different both in the viscous boundary layer and in the outer vortical region near the lee plane. This should not be surprising as we do not expect the viscous behavior to scale conically, i.e., as $\delta(x,\phi)$. Moreover, for large incidence angles, there appears to be a much more significant influence of the initial conditions.

The boundary conditions at the surface, $\eta=0$, are $u=v=w=0$ and $T=T_w$. At the outer shock wave, $\eta=1$, the Rankine-Hugoniot conditions apply.

Mass conservation:

$$(u_1-\rho u)\delta_\xi+(1/r)(w_1-\rho w)\delta_\phi-(v_1-\rho v)=0 \tag{5a}$$

Tangential momentum:

$$(w_1-w)+(1/r)\delta_\phi(V_1-V)=0 \tag{5b}$$

$$(u_1-u)+\delta_\xi(V_1-V)=0 \tag{5c}$$

Normal momentum:

$$\rho=\frac{\gamma+1}{\gamma-1+(2/M_{n_1}^2)} \tag{5d}$$

where subscript 1 denotes freestream components at the shock wave and M_{n1} is the freestream normal Mach number which is a function of δ_ξ, δ_ϕ. The four Eqs. (5a-d) coupled with the continuity Eq. (1a) evaluated at the half-point $\eta=1-(\Delta\eta/2)$ give five equations for the five unknowns u, v, w, ρ, δ_ξ. The direction cosine δ_ϕ is treated iteratively with the shock values for p and T, which are only functions of M_{n1} from the Rankine-Hugoniot conditions. The coupled u, v, w boundary conditions are incorporated implicitly into the CSIP algorithm. The combination of the Rankine-Hugoniot conditions and the coupled continuity equation ensure that global mass conservation is maintained. The final form of the outer boundary conditions includes Eq. (5b), which is linear since δ_ϕ is treated explicitly, and with Eqs. (5a), (5c), and (5d) combine to give

$$\begin{aligned}&\tfrac{1}{2}M_\infty^2[1-(u_1u+v_1v+w_1w)][(\gamma-1)\\&-2\gamma(u,u+v,v+w,w)+(\gamma+1)(u^2+v^2+w^2)]\\&=[1-2(u_1u+v_1v+w_1w)+(u^2+v^2+w^2)]\end{aligned} \tag{5e}$$

In this form the streamline solution, appearing in the original system, has been eliminated. The system Eqs. (5) is quasilinearized in the same manner as that for the interior equations.

All the CSIP and SIP calculations were convergent at least to 10^{-6} for the L_2 norm for incidence angles $\alpha\le 45$ deg. The pressure equation is converged at least to 10^{-7} for $\alpha/\theta<3.2$. For $\alpha/\theta\ge 3.2$, the pressure solution exhibits a slow divergence that apparently is associated with the explicit or uncoupled character of the normal momentum equation. If the pressure field is under-relaxed by including a time-like term in the normal momentum and energy equations, this divergence is suppressed and the overall system converges; however, the under-relaxation is very expensive computationally and it is evident that coupling the pressure directly would be more desirable.

Finally, symmetry conditions $u_\phi=v_\phi=T_\phi=p_\phi=0$ and $w=0$ (or $w_{\phi\phi}=0$) are imposed at the lee and wind planes. These conditions are coupled implicitly into the CSIP and SIP algorithms by appropriately modifying the coefficients of the difference equations at these locations; e.g., $u_{k+1}=u_{k-1}$ at $k=1$, therefore, $S_{\hat{u}_{j,k}}=0$ in Eqs. (3a) and (3b) and $N_{\hat{u}_{j,k}}$ is modified to include the U_{k+1} coefficient so that $N_{\hat{u}_{j1}}=N_{\hat{u}_{j1}}+S_{\hat{u}_{j1}}$, etc. The effect of relaxing the symmetry conditions to evaluate possible vortex shedding at larger incidence has not been considered here.

VI. Pressure Interaction and Departure

For each sweep of a one-step or global relaxation procedure the appropriate treatment of the pressure interaction term p_x in the axial momentum equation (1b) is essential. Even for supersonic freestreams an "elliptic" pressure interaction is transmitted upstream through the p_x term when regions of subsonic flow, as in the wall boundary layer, are present. If p_x is prescribed, the equations are truly parabolic and the upstream effect is lost. However, for flows where upstream effects are significant, if the p_x term is backward differenced in any form the interaction is included in the system.[2,8] This is manifested in the appearance of departure curves or "instabilities" whenever $\Delta x\le(\Delta x)_{\min}$ (Refs. 10 and 11); where $(\Delta x)_{\min}$ is of the order of the thickness of the subsonic layer or $O(Re^{-1/2})$ for the viscous cone flow.[2] Therefore, in the present application, with $Re\gg 1$, reasonably accurate solutions are possible even for $\Delta x\approx(\Delta x)_{\min}$.

This procedure is, however, inconsistent and for flows with significant pressure interaction may be inadequate. A global relaxation procedure is required if the inconsistency is to be eliminated. Moreover, in the global procedure it is necessary that each marching sweep be departure free and yet allow for an implicit pressure interaction in order to circumvent the separation point singularity that arises with an explicit pressure representation. In an earlier incompressible PNS thin layer study,[2,8] it was shown that only forward p_ξ differencing is departure free and stable globally. With this approximation it is possible to march through axial separation regions. This procedure was also tested here for the cone calculations and the earlier conclusions obtained both analytically and numerically were verified. Although this effect is relatively unimportant for cone flows where solutions with $\Delta x>(\Delta x)_{\min}$ are acceptable except very close to the tip, for more complex configurations, and where axial separation occurs, this procedure is considered extremely important and will be the basis of further analysis. The following tests were performed here for both single and multiple global sweeps: 1) p_ξ backward differenced; 2) p_ξ central differenced and 3) p_ξ forward differenced. Results are shown in Table 1 for the heat transfer for 0 and 5-deg incidence angles. From these results, it would appear that forward differencing for p_ξ leads to a solution that approaches the backward differenced value as the number of global iterations becomes large; the difference in the two results is rather small and appears to be $O(\Delta\xi)$. As predicted analytically for incompressible flow, the global iteration procedure for compressible flow, with forward differencing for p_ξ, is stable; however, the convergence rate is somewhat slow. This would appear to be a topic for future consideration.

For the cone calculations, detailed tests for the value of $(\Delta x)_{\min}$ as a function of Re have been considered. The

Table 1 Heat transfer results for 0- and 5-deg incidence angles

q(wind plane) / $q\left(\alpha=0, \frac{\partial}{\partial\xi}=0\right)$ Wind plane	w, $\xi=63$ cm, Tracy conditions ($\Delta\xi=3$ cm) (51 × 51 grid)		
		$\alpha=0$ deg	$\alpha=5$ deg
$p_\xi=0$ is the downstream boundary condition	p_ξ = backward	1.082	1.761
	p_ξ = forward 1st global sweep	0.963	1.712
	p_ξ = forward 35th global sweep	1.053	1.753

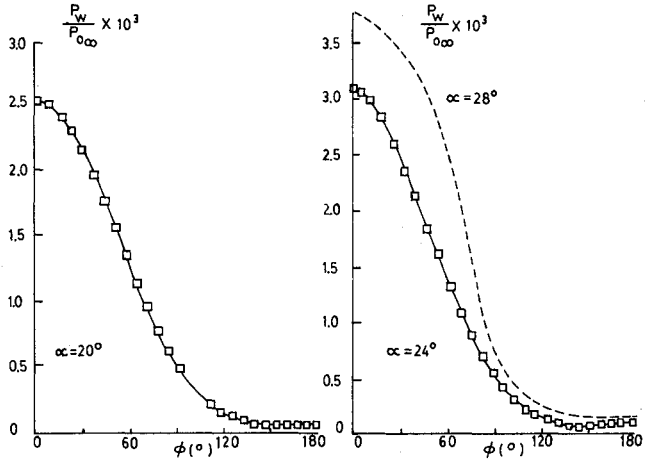

Fig. 3 Surface pressure at large incidence for Tracy conditions.

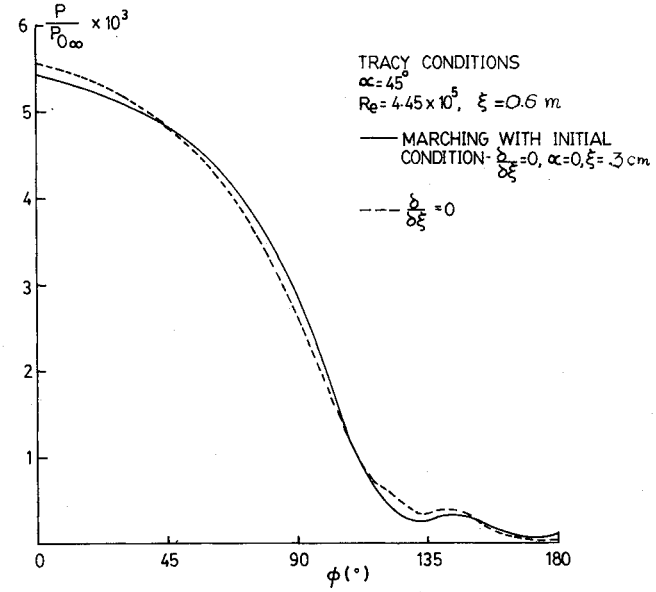

Fig. 4 Surface pressure at very large incidence—effect of initial conditions.

limiting step size $(\Delta x)_{\min}$ is proportional to the thickness of the subsonic region $(y_{M=1})$ and this is maximum at the lee plane. These results confirm the earlier analyses,[2,8] which also predicted that $(\Delta x)_{\min}/y_{M=1}$ decreases as Re increases. A stability curve is given in Ref. 6. Finally, we recall that the p_η contribution to p_x is treated implicitly and with a backward or marching mode for v_ξ; therefore, the entire global interaction is contained in p_ξ.

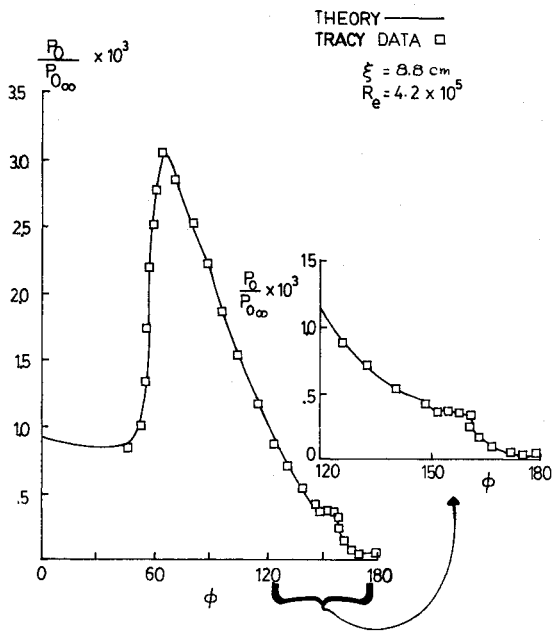

Fig. 5 Stagnation pressure; $Y=0.51$ cm, $\alpha=20$ deg.

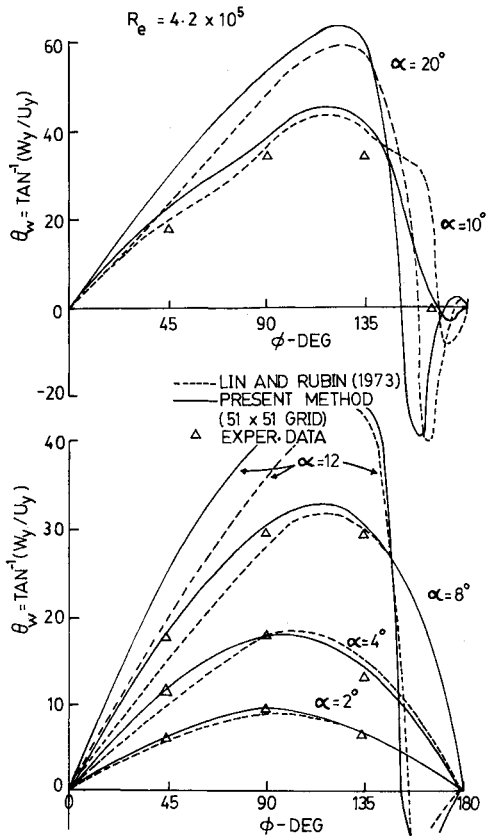

Fig. 6 Surface streamline inclination—moderate incidence (Tracy conditions).

VII. Results

Solutions have been obtained for two flow conditions for which experimental data is available.[7,9] Uniform grids were specified in η and ϕ. Calculations were run with both relatively coarse grids, e.g., 10×21, 19×31, and several finer grids. For a 51×51 grid, calculation times were 0.0008 s/CSIP iteration/grid point on the AMDAHL 470 computer. On the order of 7-15 CSIP iterations are required to converge the (u, v, w, δ_ξ) system for the low angle of attack, and about 80 for the large angle of attack for a given δ_ϕ and p_ϕ.[6]

Table 2 Surface streamline inclination, $\tan^{-1}(w_y/u_y)|_{y=0}$

	ϕ, deg	0	22.5	45	67.5	90	112.5	135	157.5	180
$\alpha=7$ deg, $M_\infty=10$, $\theta=10$ deg	Jones (inviscid)	0	1.732	3.284	4.583	5.517	5.851	5.385	3.502	0
	Lin and Rubin[12]	0	1.726	3.291	4.601	5.533	5.870	5.390	3.471	0
	Present method (55 × 51 grid)	0	1.722	3.288	4.598	5.531	5.872	5.392	3.497	0
$\alpha=11$ deg, $M_\infty=10$, $\theta=10$ deg	Jones (inviscid)	0	2.667	5.333	7.017	9.217	9.300	10.300	7.239	0
	Lin and Rubin[12]	0	2.830	5.701	7.889	9.650	10.619	11.090	8.050	0
	Present method (55 × 51 grid)	0	2.894	5.852	8.113	9.938	10.908	11.486	8.494	0

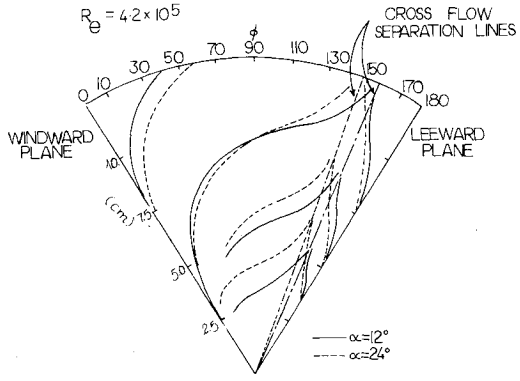

Fig. 7 Surface streamline patterns, $\alpha = 12, 24$ deg (Tracy conditions).

Marching solutions have been obtained for incidence angles (α) up to 45 deg on a 10-deg half-angle (θ) cone or $\alpha/\theta \approx 4.5$, and "conical" solutions with $\partial/\partial\xi = 0$ have been obtained for the same configuration for $\alpha/\theta \approx 5.4$.

Excellent agreement with data[6] was obtained for the heat transfer at the wind and lee planes[4] as well as for the pressure distribution (Figs. 3 and 4). The effect of the imbedded secondary flow shock wave is apparent only for the largest incidence angles.

The effect of embedded secondary shock can be seen somewhat more clearly in the pitot pressure profile of Fig. 5. The significant change in p_0 across the shock layer can be discerned. The stagnation pressure is affected by the inclination of the outer shock, the growth of the boundary layer, secondary flow separation, and the appearance of imbedded shock waves; however, the static pressure is approximately constant in the surface boundary layer. Near the wind plane, both p and p_0 are essentially invariant. However, as is seen in the following figures, the secondary flow patterns away from the wind plane are extremely complex and include all of the phenomena alluded to previously. Additional p, p_0, and heat transfer results are given in Ref. 6.

The surface streamline inclination and flow patterns (Figs. 6 and 7 and Table 2) reflect the occurrence of secondary flow separation and for the largest incidence angles a double separation effect is obtained. This phenomena has been seen experimentally in turbulent flows and by Marcillat[9] for laminar flows, but has not been reported in earlier numerical studies. In view of the relatively coarse (51 × 51 uniform) grid we reserve comment on the interpretation of the present results; however, the very existence of a converged double separation solution, as obtained here, raises several questions concerning the sensitivity and influence of the initial conditions, and in particular the conical flow approximation close to the cone tip for large α. One test case, for a 181 × 181 grid and $\alpha \approx 45$ deg, that was not run to convergence due to the computer costs, did not indicate a significantly different vortex pattern; therefore, it is conjectured that increased resolution will not eliminate the double vortex. The question of initial conditions will be discussed shortly.

The primary separation point is relatively insensitive to incidence for large α as is seen in Fig. 8. As in all earlier calculations, the present analysis predicts the onset of separation for $\alpha \approx 7$-8 deg. The separated regions found by Marcillat[9] for $\alpha > 4$ deg are not recovered here. The location of the primary vortex center is defined as the point where the secondary flow velocity is zero and is discussed in more detail in Ref. 6. The vortex moves away from the surface for increasing α, but appears to asymptote to a fixed location, at a given value of η relatively close to the shock, of $\alpha > 30$ deg. For $\alpha \leq 30$ deg, the "inviscid" solution in the outer portion of the shock layer, including the vortex location, is approximately independent of ξ and a function only of η and ϕ, i.e., conical-like flow behavior is observed in the outer region for moderate incidence.

The boundary and imbedded shock pattern are seen in Fig. 9. The imbedded shock increases in strength and the outer shock shape begins to deviate significantly from the near circular pattern of smaller incidence angles. The flow is supersonic over most of the range of ϕ for $\alpha > 12$ deg.[6] Although the sonic lines are represented accurately, the captured internal shock is represented only with an accuracy of ± 3 deg in ϕ since this is not a sharp interface. The shock standoff δ near the lee plane first exhibits a range where $\delta_\phi < 0$ for $\alpha \approx 28$ deg. w is positive on both sides of the imbedded shock in the region, where $\delta_\phi < 0$. At the point ϕ_p, where $\delta_\phi = 0$, the shock is primitive. This implies that from this point to the lee plane, most of the shock strength comes from the decrease in the u velocity. Therefore, in the region $\phi > \phi_p$, $(\delta_\xi)_\phi$ is much greater than for $\phi \leq \phi_p$. It might be expected that with such a large δ_ξ, far downstream, the shock pattern will revert to $\delta_\phi \geq 0$ everywhere. With the conical initial conditions, the marching solutions for large α do show some axial variations, but for $\xi < 63$ cm a region with $\delta_\phi < 0$ persisted.

A description of the secondary flow is given for Tracy's conditions and $\alpha = 45$ deg, in Fig. 10. Those solutions, with a 51 × 51 grid, are converged to the tolerances described earlier. This pattern is also obtained in the initial conditions with $\partial/\partial\xi = 0$ and with marching for step conditions for $\xi \geq 63$ cm. The strong imbedded shocks, the double vortex pattern, and the "apple"-like shape of the outer shock boundary are particularly unusual. These solutions indicate that, for large α, the region of $\delta_\phi < 0$ becomes more pronounced. As was noted previously, $\delta_\phi < 0$ is not a stable feature (in the marching calculation), and far downstream we expect that $\delta_\phi \geq 0$ may be recovered.

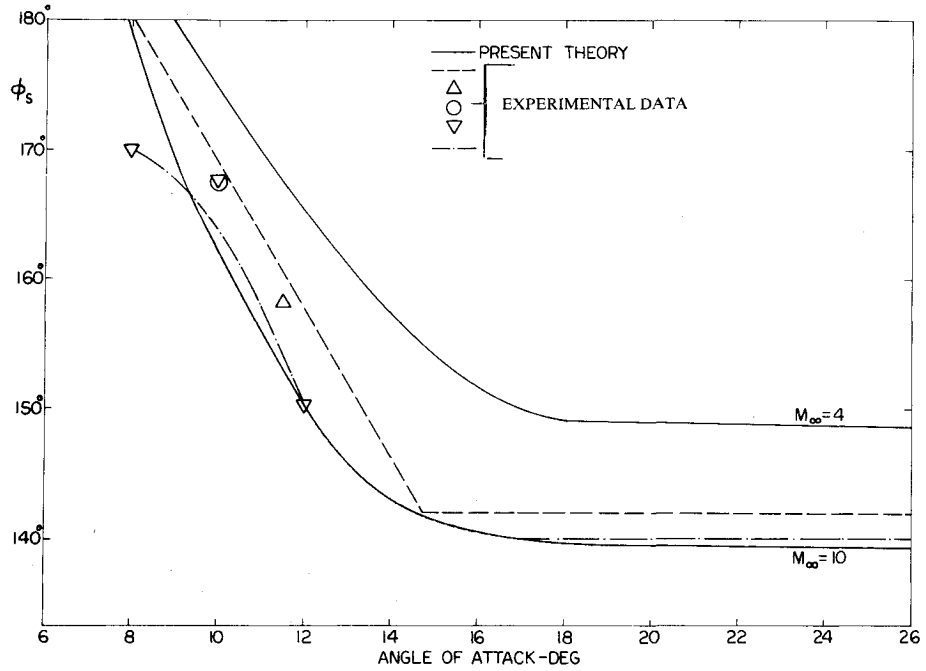

Fig. 8 Primary separation point location.

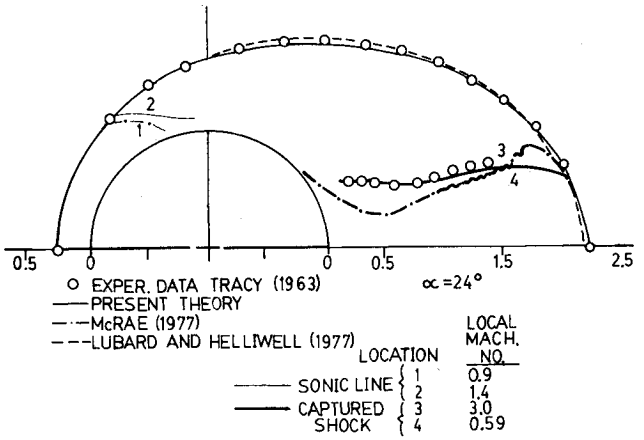

Fig. 9 Shock and sonic line patterns for $\alpha = 24$ deg.

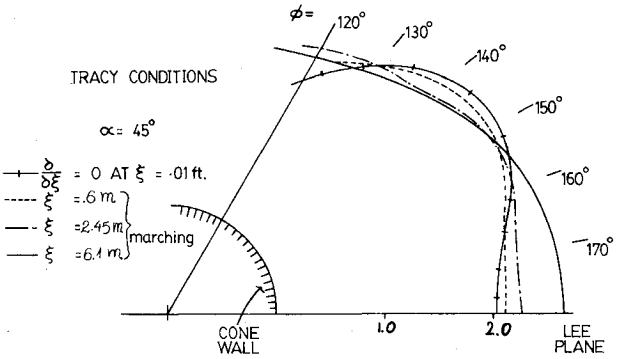

Fig. 11 δ/r near the lee plane for large incidence.

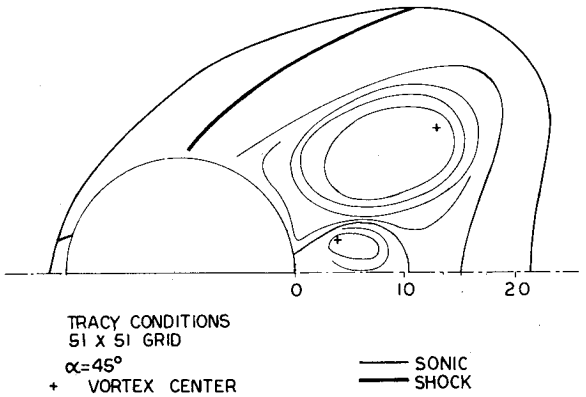

Fig. 10 Flow pattern for $\alpha = 45$ deg.

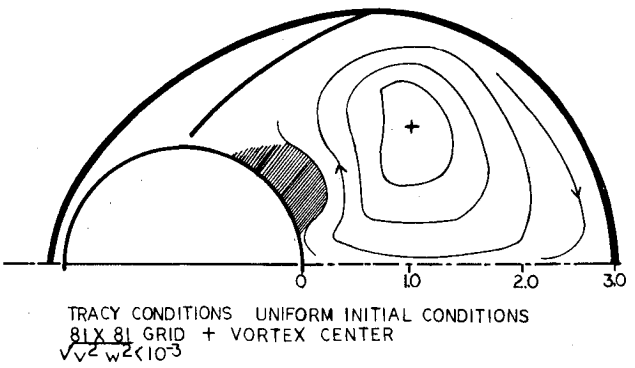

Fig. 12 Flow pattern for $\alpha = 45$ deg, $\xi = 305$ cm.

For $\alpha = 54$ deg, the normal shock Mach number for most of the region near the lee plane was very close to 1. This result is indicative of the behavior of the cone flow at very large angle of attack, i.e., the shock appears to asymptote to a sonic line near the lee plane. As α increases further the shock may eventually detach from the cone tip. Values of $\alpha/\theta > 5.4$ were not considered.

Returning to double vortex pattern and the occurrence of $\delta_\phi < 0$ in the cross plane for high angle of attack, it is hypothesized that this phenomena may be associated with the initial conditions, e.g., the conical flow condition $\partial/\partial\xi = 0$ at a cross section very close to the cone tip. Since the viscous terms preclude the existence of a conical solution to the present problem, the combined effect of small r or small Reynolds number and large α, at the initial station where uniform or conical conditions are imposed, may lead to the double vortex pattern. Since the outer inviscid region is hyperbolic, for large α, these initial conditions may persist for

large distances downstream. Figure 11 attempts to demonstrate this effect in a very approximate sense. For $\alpha = 45$ deg the calculation was continued beyond $\xi = 63$ cm by marching with very large values of $\Delta\xi$. Figure 12 describes the value of δ/r near the lee plane (120 deg $\leq \phi \leq$ 180 deg) for different ξ locations. It is seen that for $\xi > 4.65$ m, δ_ϕ becomes positive everywhere. This result is in agreement with the discussion concerning the long-range effect of the initial conditions. Figure 12 depicts an 81×81 converged solution far downstream of the cone tip for $\alpha/\theta = 4.5$. Uniform rather than conical conditions were assumed at the location $\xi = 3$ mm. It is seen that only one vortex now exists near the lee plane. The vortex center is also located closer to the cone wall than was found with the solutions nearer to the cone tip. A region, between the vortex and the cone wall, with very small cross flow velocities, $O(10^{-3})$, can be identified by the shaded area in Fig. 12. The shock configuration near the lee plane is also different from the conical solution ($\xi = 248$ cm) described in Fig. 11. These results are indicative of the sensitivity of the present solutions to both initial conditions and distance from the cone tip. The influence of the initial conditions is discussed further in Ref. 6.

In summary, the CSIP procedure described here captures shocks, predicts vortex lift-off, multiple separation regions, and complex shock patterns. The possible suppression of departure effects with global iteration and forward p_ξ differencing and the adequacy of single sweep backward differencing for conical flows with small subsonic viscous layers has been demonstrated. The accuracy and flow stability of the present solutions and the importance and persistence of initial conditions for very large incidence remains a question for future study.

Acknowledgments

The authors would like to thank Professor P. K. Khosla for many helpful discussions. This research was supported by the Office of Naval Research under Contract N00014-79-C-0849, Task No. NR 061-258.

References

[1] Davis, R. T. and Werle, M. J., "Numerical Methods for Interacting Boundary Layers," *Proceedings of the 1976 Heat Transfer and Fluid Mechanics Institute*, Stanford University Press, 1976.

[2] Rubin, S. G., "A Review of Marching Procedures for Parabolized Navier Stokes Equations," Symposium on Numerical and Physical Aspects of Aerodynamic Flows, California State Univ., Long Beach, Calif., Jan. 1981 (Proceedings by Springer Verlag).

[3] Davis, R. T. and Rubin, S. G., "Non-Navier Stokes Viscous Flow Computations," *Computers and Fluids*, Vol. 8, March 1980, pp. 101-131.

[4] Lin, T. C., Rubin, S. G., and Widhoph, G., "Two Layer Model for Coupled Three Dimensional Viscous and Inviscid Flow Calculations," AIAA Paper 81-0118, Jan. 1981.

[5] Rubin, S. G. and Khosla, P. K., "Navier Stokes Calculations with Coupled Strongly Implicit Method. Part I: Finite Difference Solution," AIAA Paper 79-0011, 1979; also, *Computers and Fluids*, Vol. 9, June 1981, pp. 163-180.

[6] Lin, A. and Rubin, S. G., "Three-Dimensional Supersonic Viscous Flow Over a Cone at Incidence," Dept. of Aerospace Engineering and Applied Mechanics, Univ. of Cincinnati, Cincinnati, Ohio, Rept. AFL-81-9-57, Nov. 1981.

[7] Tracy, R. R., "Hypersonic Flow Over a Yawed Circular Cone," California Institute of Technology, Aeronautical Lab., Memo. 69, 1963.

[8] Rubin, S. G. and Lin, A., "Marching with the PNS Equations," *Proceedings of the 22nd Israel Annual Conference in Aviation and Aeronautics*, Tel-Aviv, Israel, 1980, p. 60; also, *Israel Journal of Technology*, Vol. 18, March 1981.

[9] Marcillat, J. and Roux, B., "Experimental and Theoretical Study of Supersonic Flow Over a Yawed Circular Cone," *AIAA Journal*, Vol. 10, Dec. 1972, pp. 1625-1630; also, Marcillat, J., Doctoral Thesis, Universite de Province, Marseille, France, July 1970.

[10] Lubard, S.C. and Helliwell, W. S., "An Implicit Method for Three Dimensional Viscous Flow with Application to Cones at Angle of Attack," *Computers and Fluids*, Vol. 3, March 1975, pp. 83-101.

[11] Lin, T. C. and Rubin, S. G., "Viscous Flow Over a Cone at Moderate Incidence. I: Hypersonic Tip Region," *Computers and Fluids*, Vol. 1, Jan. 1973, pp. 37-57.

[12] Lin, T. C. and Rubin, S. G., "Viscous Flow Over a Cone at Moderate Incidence. II: Supersonic Boundary Layer," *Journal of Fluid Mechanics*, Vol. 59, March 1973, pp. 593-620.

[13] McRae, D. S., "A Numerical Study of Supersonic Viscous Cone Flow at High Angle of Attack," AIAA Paper 76-77, 1976.